processes

MDPI

Article

Paraquat Removal from Water by Magnetic Nanoparticles Coated with Waste-Sourced Biobased Substances

Santiago Ocampo [1], María Eugenia Parolo [2] and Luciano Carlos [1,*]

[1] Instituto de Investigación y Desarrollo en Ingeniería de Procesos, Biotecnología y Energías Alternativas, PROBIEN (CONICET-UNCo), Universidad Nacional del Comahue, Buenos Aires 1400, Neuquén, Argentina; santiago.ocampo@probien.gob.ar

[2] Centro de Investigación en Toxicología Ambiental y Agrobiotecnología, CITAAC (CONICET-UNCo), Facultad de Ingeniería, Universidad Nacional del Comahue, Buenos Aires 1400, Neuquén, Argentina; maria.parolo@fain.uncoma.edu.ar

* Correspondence: luciano.carlos@probien.gob.ar

Abstract: The use of biobased substances derived from industrial and household waste as renewable raw materials for environmental applications is gaining prominence due to its sustainable and cost-effective approach to waste valorisation. Herein, we report the uptake of paraquat, a widely used pesticide, by magnetite nanoparticles coated with composted urban biowaste-derived substances (MNP-BBS). The magnetic nanoparticles were prepared using a modified co-precipitation method, and were characterized through various physicochemical techniques. They were tested as an adsorbent for paraquat removal under diverse experimental conditions, exploring the influence of pH (3–10), MNP-BBS dosages (200–1000 mg L^{-1}), ionic strength (0–0.01 M), and presence of organic matter. The kinetic study revealed that the adsorption of paraquat onto MNP-BBS follows the pseudo-second-order model, reaching the adsorption equilibrium after 2 h of contact and 90% of paraquat removal in the best condition tested (1000 mg L^{-1}). The equilibrium experimental data showed a high adsorption performance with a good fitting to the Freundlich isotherm model. Also, from Langmuir model a maximum adsorption capacity of 0.085 mmol g^{-1} was estimated. The results indicated that electrostatic interaction between the negative functional groups of the adsorbent and the paraquat play a major role in the adsorption mechanism, although the contribution of π-π and hydrophobic interactions cannot be completely ruled out. This research underscores the potential of utilizing MNP-BBS as an effective adsorbent for the removal of paraquat, shedding light on its application in sustainable water purification processes.

Keywords: nanotechnology; magnetite nanoparticles; adsorbents; water remediation; humic-like substances; paraquat

check for updates

Citation: Ocampo, S.; Parolo, M.E.; Carlos, L. Paraquat Removal from Water by Magnetic Nanoparticles Coated with Waste-Sourced Biobased Substances. *Processes* **2024**, *12*, 1339. https://doi.org/10.3390/pr12071339

Academic Editors: Natalia Quici, Víctor Nahuel Montesinos and María de los Milagros Ballari

Received: 8 May 2024
Revised: 11 June 2024
Accepted: 25 June 2024
Published: 27 June 2024

1. Introduction

Since pesticides are crucial substances used to protect plants from pests and ensure the quality of harvests, their application has been a routine practice in agriculture [1,2]. Unfortunately, the excessive use of pesticides has caused environmental pollution and has been linked to chronic health problems in the population [3]. Paraquat (PQ) is a broad-spectrum, non-selective and very fast-acting herbicide, which acts on the foliage causing cell death and desiccation of the green tissue [4]. The great versatility of PQ led to its excessive use in several regions, but due to its level of acute toxicity, many countries have suspended its application. However, it is still widely used in the United States, Asia, and Latin America [5]. PQ can cause severe damage to human organs, in some cases leading to death, due to ingestion or skin exposure [6]. Its main health consequences are related to severe lung failure, although it has also been linked to several diseases in humans, including Parkinson's disease [6]. In light of that, it is imperative to remove PQ from the aquatic systems and purify the water resources. Among traditional methods for the treatment of pesticides in water, technologies based on adsorption processes are considered the most promising due to their simple design and operation, cost-effectiveness, and potential for regeneration of adsorbents. In this sense, nanomaterials have enormous potential for the efficient removal of chemical and biological contaminants. This potential is due to the fact that thanks to their nanometric dimensions, all of these materials have a very high surface/mass ratio, which gives them high adsorbent capacities and high reactivity [7]. Consequently, in the last decades magnetic nanoadsorbents have emerged as a new generation of materials for water treatment as they provide a convenient approach to separate and remove contaminants through the application of a magnetic field [8,9]. Magnetic separation overcomes many of the problems present in filtration, centrifugation, or gravitational separation, and generally requires less energy to achieve a given level of particle separation in aqueous media [9]. Iron oxides (magnetite or maghemite) nanoparticles are commonly used as magnetic adsorbents and their coating with different materials, such as polymers, silica, and carbonaceous materials, yields nanomaterials with improved stability in water and improved surface adsorption properties towards a target pollutant [10]. Ananpattarachai et al. [11] reported that composites of activated carbon and iron oxide nanoparticles with a surface area close to 760 m^2 g^{-1} are effective adsorbents to remove PQ from aqueous solution. On the other hand, Fernandes et al. [12] found that magnetic adsorbents composed of magnetite cores functionalized with bio-hybrid siliceous shells presents a high PQ removal performance with an adsorption capacity of 257 mg g^{-1}.

In order to reduce the cost associated to the adsorption process, low-cost materials from natural sources, industrial wastes, and agriculture remnants have been studied as adsorbents in water purification processes [13–15]. In particular, the transformation of diverse industrial and agriculture waste streams into adsorbent materials has garnered significant attention, owing to its potential as a sustainable method of waste valorization [13,16]. For instance, activated carbon derived from used tires was shown to be an effective and rapid adsorbent for removing paraquat from aqueous solutions [17]. In other study, Damdib et al. [18] used corn husks as the carbon precursor and synthesized magnetic biochar with microporous and mesoporous structures for the removal of PQ. These materials showed high adsorption capacity of PQ (34.97 mg g^{-1}) in synthetic water and good reusability performance after fiver cycles. In previous research of our group, magnetite nanoparticles coated with bio-based substances (BBS) derived from urban public park trimming and home gardening residues were employed as sustainable and reusable magnetic adsorbents for the removal of various inorganic and organic contaminants [19–21]. These nanoparticles exhibited remarkable versatility as adsorbents, removing a wide variety of contaminants with high efficiency. Nonetheless, it is noteworthy that the adsorption capacity specifically against pesticides was not evaluated. The BBS have been found to be mixtures of molecules of different molecular weight (from 67 to 463 kg mol^{-1}) that are composed of aliphatic C chains substituted by aromatic rings and various functional groups such as COOH, CON, CO, PhOH and O-alkyl, among others [21]. These different types of chemical groups capable of interacting with organic and inorganic compounds, make BBS good candidates as adsorbents of contaminants in aqueous media. Based on these considerations, the present work focuses on obtaining magnetite nanoparticles coated with BBS with PQ adsorption properties for a future application as nanomaterial sorbents for decontamination. The synthesis and structural characterization of BBS-nanoparticles is firstly presented, followed by an evaluation of the PQ adsorption properties. Special attention is paid to the effects of pH, dosage and ionic strenght on the adsorption, which could be used to optimize the performance of BBS-nanoparticles as a PQ adsorbent.

2. Materials and Methods

2.1. Materials

$Fe_2(SO_4)_3xnH_2O$, $FeCl_2x4H_2O$, NaOH, H_2SO_4, $CaCl_2$, and paraquat were purchased from Sigma-Aldrich (St. Louis, MO, USA). Ammonium hidroxide (28%) and NaCl were purchased from Merk (Rahway, NJ, USA). Humic Acid (Leonardite) were obtained from the International Humic Substance Society (IHSS), Triangle Park, NC, USA. The bio-based substances (BBS) utilized in this investigation were obtained through a 180-day composting process of green waste at the Acea Pinerolese plant in Pinerolo, Torino, Italy, and subsequently processed at the pilot plant of Studio Chiono e Associati in Rivarolo Canavese, Torino, Italy. In summary, 50 g of green compost underwent treatment with 1 L of 6 M NaOH aqueous solution while being stirred at 60 °C for 4 h. Following the reaction, the mixture was separated via centrifugation. The supernatant was subsequently concentrated and different fractions were then isolated using a lab-scale ultrafiltration unit equipped with a membrane featuring a molar mass cut-off of 5 kDa. The retained fraction obtained was subsequently dried at 60 °C for 24 h. The resultant BBS constituted approximately 20–30% of the initial compost mass. Details regarding the chemical composition of the BBS can be found elsewhere [20,22].

2.2. Synthesis of Magnetic Nanoparticles

To obtain the magnetite nanoparticles coated with bio-based substances (MNP-BBS), a variation of the co-precipitation method described in the literature was used [21]. The synthesis procedure is summarized below: 4.7 g of $Fe_2(SO_4)_3{\cdot}nH_2O$ and 3.0 g of $FeCl_2{\cdot}4H_2O$ were dissolved in 100 mL of distilled water. The solution was introduced into a single-neck flask and heated to 90 °C using an external bath. Upon reaching the desired temperature, 10 mL of NH_4OH were added, followed immediately by the addition of 50 mL of a BBS solution (10 g L^{-1}). The system was maintained at 90 °C and subjected to magnetic stirring for 30 min. Subsequently, the dispersion was cooled to room temperature. The resulting black solid was washed with distilled water and separated from the supernatant using a magnet. This washing process was repeated four times to ensure thorough removal of impurities. Finally, the obtained product was dried for 12 h in an oven set at 80 °C. The nanoparticles thus obtained were subsequently ground and stored in a dark glass container.

2.3. Characterization Techniques

Fourier transform infrared (FTIR) spectra were recorded on an Infralum FT-08 transmission spectrophotometer equipped with a DLATGS detector (Lumex, Wakendorf II, Germany). The resolution used was 4 cm^{-1} with 60 scans in the range of 5000–400 cm^{-1}. KBr pellets were used (sample concentration 0.6% *w*/*w*). X-ray diffraction (XRD) patterns were obtained using a DII diffractometer (Riguku, Tokyo, Japan) equipped with a Cu Kα source, a horizontal Bragg–Brentano geometry in a flat sample-holder, with 2θ step of 0.05° in the 2θ range of 25–70°. The average crystallite size was estimated using the Scherrer equation. For the calculation, the peak with the highest intensity was selected. High-resolution transmission electron microscopy (HRTEM) measurements were performed on a JEM 3010 UHR microscope (JEOL Ltd., Tokyo, Japan) (300 kV acceleration, LaB6 filament). For sample preparation, a few drops of a previously sonicated aqueous MNP-BBS suspension were placed on carbon-coated copper pierced grids and allowed to dry prior to analysis. Particle cluster size (dz) were measured on aqueous dispersions of magnetite nanoparticles by dynamic light scattering using a Zetasizer Nano Series (Malvern Instruments, Worcestershire, UK) with a He–Ne laser (633 nm). Hydrodynamic diameters were deduced using the Stokes–Einstein equation.

2.4. Adsorption Experiments

Kinetic experiments were conducted contacting MNP-BBS (200–1000 mg L^{-1}) with a 3 mg L^{-1} PQ solution at pH 6.2. The pH was adjusted to the desired value by adding small amounts of NaOH or H_2SO_4 as appropriate. Sampling was performed at predetermined times up to a maximum of 6 h. Subsequent to the contact period, a 5 mL aliquot was withdrawn and the solid was magnetically separated from the solution. The magnetic separation process was carried out by placing 5 mL of sample in a 25 mL container (R = 10 mm, h = 40 mm) that was on a neodymium magnetic disk (20 × 10 mm, diameter × height). After 10 min, a defined volume of the supernatant was withdrawn for analysis. In cases where the pH of the medium was higher than 7, magnetic separation times of 24 h were applied to achieve a good separation process. The concentration of PQ in the supernatant was determined using a UV-Vis spectrophotometer following the absorbance at 258 nm. Furthermore, experiments were conducted to elucidate the influence of operational parameters such as pH, ionic strength, adsorbent dosage, and the presence of organic matter in the solution on the performance of PQ removal. The uptake at a certain time, q_t (mg g^{-1}), and the % *Removal* were determined using the following equations:

$$q_t = \frac{(C_0 - C_t) \times V}{m} \tag{1}$$

$$\%\ Removal = \frac{(C_0 - C_t) \times 100}{C_0} \tag{2}$$

where C_0 and C_t represent the PQ concentration (mg L^{-1}) at time 0 and t (min), respectively, V denotes the volume (L) of the solution, and m the mass (g) of the adsorbent. PQ adsorption isotherm was obtained at room temperature and pH 6.7, with a 500 mg L^{-1} suspension of MNP-BBS, varying the initial concentration of PQ from 1 to 75 mg L^{-1}.

The data were fitted to Langmuir and Freundlich adsorption models. The Langmuir model is based on the assumption of monolayer adsorption on the adsorbent surface, finite adsorption capacity for the adsorbate, and the occupation of a single site per each molecule of absorbate. The Langmuir model is expressed as:

$$q_e = \frac{q_{max} \times K_L \times C_e}{1 + K_L \times C_e} \tag{3}$$

where q_e is the adsorbed PQ at equilibrium, C_e is the PQ concentration (mg L^{-1}), q_{max} is the maximum adsorption capacity and K_L is the equilibrium constant (L mg^{-1}).

The Freundlich isotherm states that the adsorption phenomenon takes place on heterogeneous surfaces and assumes that the surface sites of the adsorbent possess varying binding energies. Freundlich model is expressed as:

$$q_e = K_F \times C_e^{1/n} \tag{4}$$

K_F is the Freundlich constant ((mg g^{-1})(L mg^{-1})$^{1/n}$), which indicates the relative adsorption capacity of the adsorbent, while n is the degree of dependence of adsorption with equilibrium concentration and is associated with the adsorption intensity.

3. Results and Discussion

3.1. Characterization

Figure 1 shows the TEM images of MNP-BBS. It can be seen that the MNP-BBS exhibit a fairly regular, roughly spherical morphology with an average diameter of approximately 11 nm, featuring a narrow size distribution. Additionally, these nanoparticles tend to agglomerate forming irregular clusters. The presence of an amorphous layer surrounding the nanoparticles is be attributed to organic matter (BBS) and confirms the functionalization of de magnetite nanoparticles.

The XRD pattern of MNP-BBS sample is shown in Figure 2A. The observed reflections for 2θ at 30.1°, 35.4°, 43.0°, 53.9°, 57.2°, 62.6°, 71.4°, and 74.2° match with the lattice planes (220), (311), (400), (422), (511), (440), (620), and (533) of magnetite (01-1111, ICCD database). It is important to mention that from X-ray measurements it is not possible to differentiate between the magnetite (Fe_3O_4) and maghemite (γ-Fe_2O_3) phases, since both have the same cubic structure and their lattice parameters are almost identical [23]. On the other hand, the crystallite size of the MNP-BBS determined from the Scherrer equation was 11.7 nm. This value coincides with the size obtained by the TEM images confirming that the majority of the nanoparticles are comprised of single crystals.

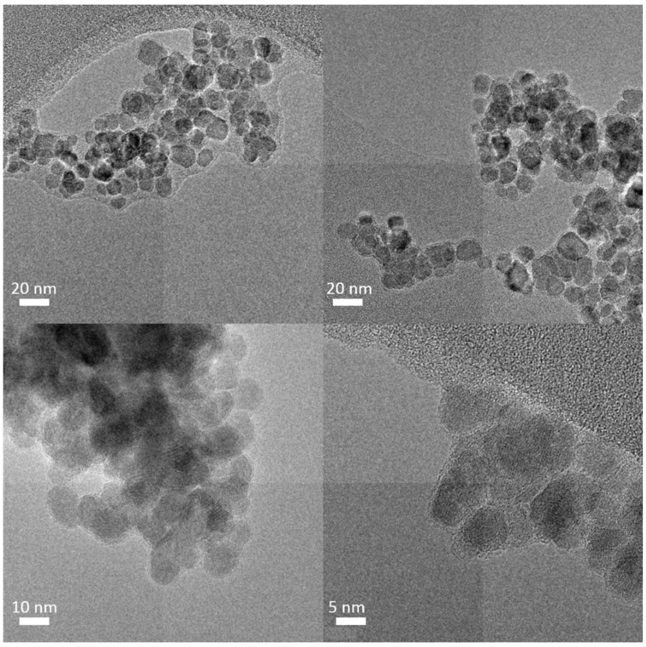

Figure 1. TEM images of MNP-BBS.

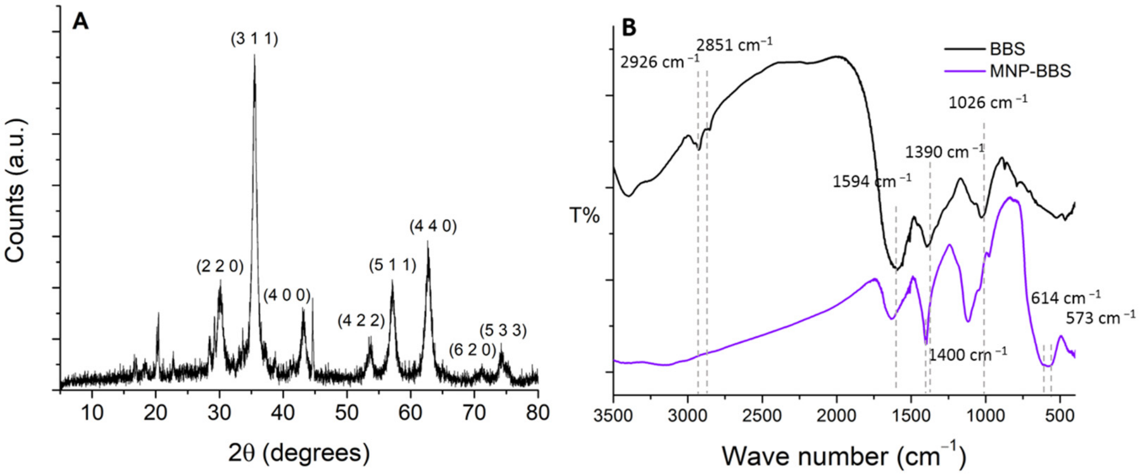

Figure 2. (**A**) XRD diffraction pattern of MNP-BBS and (**B**) FTIR spectra of MNP-BBS and BBS.

Figure 2B shows the FTIR spectra of MNP-BBS and BBS for comparison purposes. In the spectrum of BBS, the most intense bands are located at 1594, 1390, 1026 cm^{-1}, corresponding to the stretching of the C=O bond, stretching of the C–O bond of phenolic groups, and deformation of the C–O bond of polysaccharides, respectively. Likewise, lower intensity bands are observed at 2851 and 2926 cm^{-1}, associated with C–H stretching of aliphatic groups. In the case of MNP-BBS, the presence of magnetite is evident in the FTIR spectrum by the appearance of bands at 573 and 614 cm^{-1}, which are associated with the Fe–O bond, characteristic of this iron oxide [24]. Additionally, slight shifts are observed in certain bands compared to free BBS, suggesting interactions between organic matter and magnetite nanoparticles. Specifically, the intense and sharp band at 1400 cm^{-1}, reported in the literature as corresponding to the carboxylate-iron stretching [25], indicates that BBS is covalently linked to the magnetite nanoparticles via the interaction of carboxylate and the iron atoms of the surface of the magnetite nanoparticles. Furthermore, the shift of the absorption bands assigned to C–O stretching mode is typical of adsorbed carbohydrates or polysaccharide-like substances onto the iron oxide surface [26].

3.2. Aggregate Size and Magnetic Separation

Dynamic light scattering technique (DLS) was employed to ascertain the aggregate sizes of the MNP-BBS dispersion. Figure 3A display the obtained sizes for aqueous suspensions of MNP-BBS (200 mg L^{-1}) under varying pH conditions without the application of an external magnetic field. The results show an inverse correlation between the pH of the suspension and the size of the MNP-BBS aggregates, obtaining average sizes close to 1400 nm at pH 3.5, and sizes of approximately 300 nm at pH 9.1 (Figure 3A, red line). This behavior is attributed to the fact that MNP-BBS has a pH of the zero-point charge close to 3 [21] and that the abundance of negatively charged species resulting from the dissociation of acidic groups present in the BBS increases with increasing pH. Based on the DLVO theory, the stability of nanoparticles in aqueous media, and thus the degree of aggregation, results from the interplay between attractive van der Waals forces and repulsive electric double-layer interactions. As a consequence, the magnitude of the zeta potential can be used to estimate the colloidal stability of a given system; the higher the magnitude of the zeta potential, the better the colloidal stability of nanoparticles [27]. Thus, as the negative charge of the MNP-BBS increases, electrostatic repulsion intensifies, consequently leading to a reduction in aggregate size. It is noteworthy that at pH values exceeding 6, the size of the aggregates is not significantly affected by increasing pH. This could be explained considering that MNP-BBS exhibit constant zeta potential values around −30 mV at pH higher than 6 [21]. It is important to note that no sedimentation of the MNP-BBS material was observed during the first 24 h of preparation of the nanoparticle suspension at the different pHs studied, which highlights the good stability of the nanoparticle's suspension.

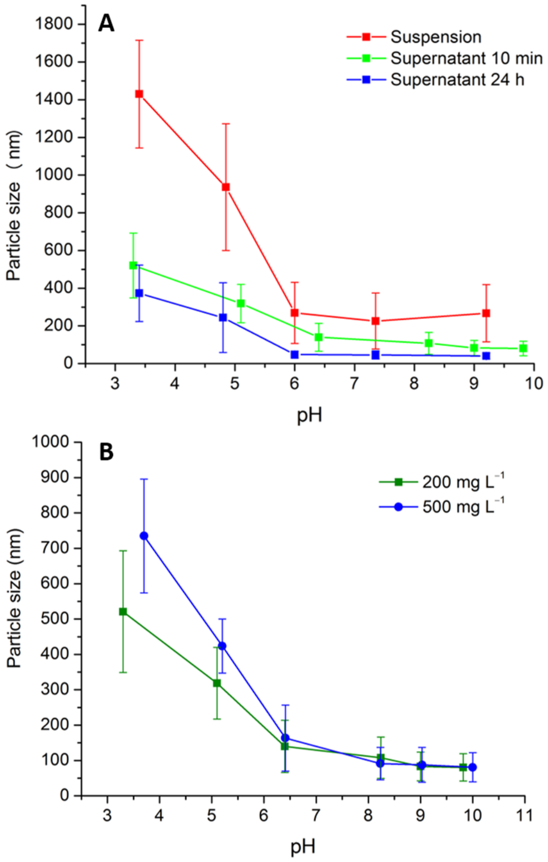

Figure 3. Aggregate size determined via DLS at different pH. (**A**) Supernatants of MNP-BBS suspensions (200 mg L^{-1}) collected at different pH without exposure to a magnetic field (red line) and after 10 min and 24 h of magnetic separation (green and blue lines, respectively). (**B**) Effect of MNP-BBS concentration (200 and 500 mg L^{-1}) on the aggregate size during 10 min of magnetic separation.

The effect of pH on the size of MNP-BBS aggregates could influence the efficiency of magnetic separation processes to remove MNP-BBS from the aqueous dispersion. Indeed, considering that the magnetic force exerted by an external magnet on the particle is proportional to the size of the particle, and that particle diffusion phenomena increase with decreasing particle size [28], it is expected that a smaller aggregate size increases the time required to achieve an effective magnetic separation. In order to obtain experimental evidence on the effect of particle size on magnetic separation, DLS analysis was performed on the supernatants of MNP-BBS suspensions collected at various time intervals after exposure to a magnetic field. Figure 3A also shows the results obtained for 10 min and 24 h of magnetic separation at different pH (lines green and blue, respectively). As expected, for longer magnetic separation times, the aggregates that persist in the supernatant after the magnetic separation are smaller; however, the observed differences are not quite significant. Also, at pH values higher than 6, negligible differences in aggregate size were observed for both conditions, and very small aggregates were measured. On the other hand, Figure 3B shows the effect of MNP-BBS concentration (200 and 500 mg L^{-1}) on the aggregate size during 10 min of magnetic separation. It can be seen that at pH values lower than 6 in the more concentrated suspension, larger aggregates remain, while at pH values higher than 6 the average size of the aggregates is the same for both concentrations. This means that the concentration of MNP-BBS does not influence the size of the aggregates remaining after 10 min of magnetic separation at pH values higher than 6. Furthermore, this indicates that smaller aggregates (lower than 100 nm) are difficult to separate with 10 min of magnetic separation.

To analyze the separation efficacy of the MNP-BSS, UV-Vis spectra of the supernatants were measured after 10 min and 24 h of magnetic separation of aqueous suspensions containing 200 mg L^{-1} of MNP-BBS at various pH values. In all cases, a decrease in the absorbance signal is observed as the pH of the medium decreases, suggesting a reduction in the concentration of MNP-BBS present in the supernatants, which in turn indicates an improvement in the magnetic separation efficiency. Likewise, a clear decrease in the absorbance signals is observed at 24 h compared to the measurements made at 10 min of separation. Figure 4 depicts the absorbance at 258 nm versus pH for the supernatant analysed at 10 min and 24 h of magnetic separation. The experimental data indicates that at pH less than 7, magnetic separation is very effective after 10 min, while at pH above 7 it is necessary to wait 24 h to achieve an efficient separation. This result shows that the efficiency of the magnetic separation process depends strongly on the degree of aggregation of the MNP-BBS.

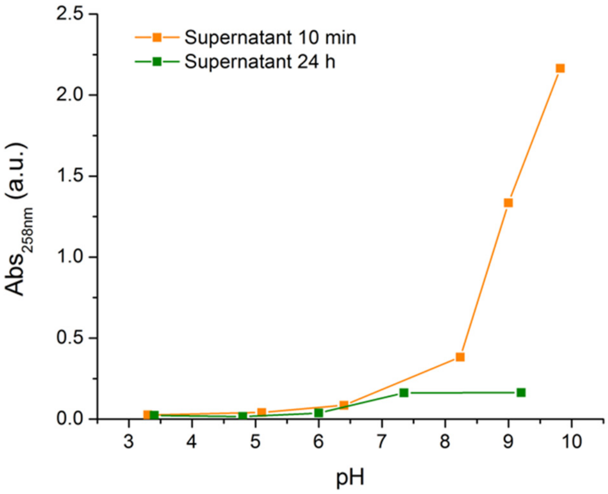

Figure 4. $Abs_{258\ nm}$ vs. pH of the supernatants after 10 min and 24 h of magnetic separation of aqueous suspensions MNP-BBS (200 mg L^{-1}).

3.3. Adsorption Experiments

Figure 5 shows the kinetic experiments of PQ adsorption at different concentrations of MNP-BBS. From these results, it is observed that after 180 min of contact time, the concentrations of PQ in solution remain practically constant, indicating that equilibrium was reached. It is important to highlight that using a concentration of 1000 mg L^{-1} of MNP-BBS, it was possible to remove 90% of PQ present in the solution. The kinetic data were fitted using the pseudo-second-order kinetic model (Equation (5)).

$$\frac{t}{q_t} = \frac{1}{kq_e^2} + \frac{t}{q_e} \tag{5}$$

where k is the pseudo-order rate constant. The values of the rate constants and the amounts of adsorbate retained at equilibrium (q_e) were determined from the nonlinear fit for each concentration of MNP-BBS (Figure 5) and are reported in Table 1.

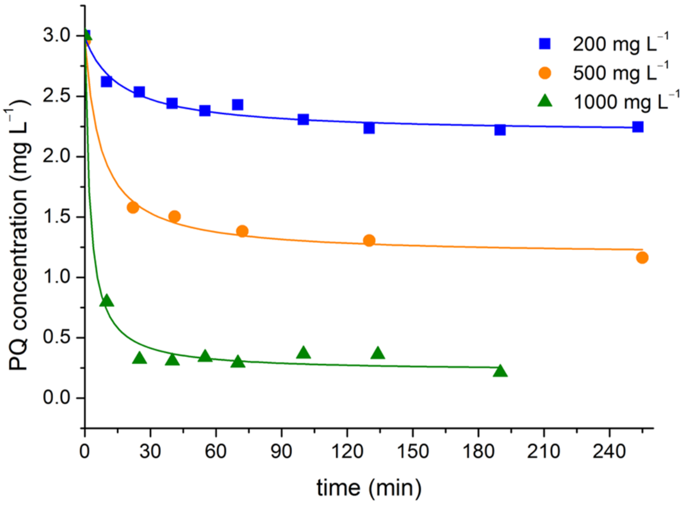

Figure 5. Kinetics profiles of PQ removal using different amounts of MNP-BBS (200–1000 mg L^{-1}). Lines represent the non-linear fit of the kinetic data using pseudo-second-order kinetic model. [PQ] = 3 mg L^{-1}, pH = 7.

Table 1. Parameters of the pseudo-second-order kinetic model for the adsorption of PQ by MNP-BBS.

Kinetic Parameters	MNP-BBS (200 mg L^{-1})	MNP-BBS (500 mg L^{-1})	MNP-BBS (1000 mg L^{-1})
q_e (mg g^{-1})	0.41	0.37	0.28
k (g mg^{-1} seg^{-1})	0.13	0.24	1.59
R^2	0.993	0.999	0.998

The effect of adsorbent dosage on PQ removal capacity was studied in the range of 200 to 1300 mg L^{-1} at pH 6.2 (Figure 6). The results show that the higher the concentration of nanoparticles, the higher the removal of PQ, reaching a removal of 90% for a dose of 1300 mg L^{-1}. On the other hand, experiments carried out varying the pH of the medium between 3 and 9 evidenced a notable increase of the % removal as pH increases (Figure 7, green line). This is accounted for PQ, a cationic species, can interact electrostatically with the anionic functional groups of the organic matter, such as the carboxylate and phenolic groups of BBS, via a cationic exchange mechanism, and therefore the magnitude of PQ binding will depend on the degree of ionization of the acid and phenolic groups [29]. As a result, the amount of PQ adsorbed on the MNP-BBS increases as the pH of the medium increases. A similar trend with pH was observed for the removal of crystal violet, a cationic dye, using similar nanoparticles [21]. It is important to note that at pH values above 7.2, a removal higher than 80% of PQ is achieved with 500 mg L^{-1} of adsorbent.

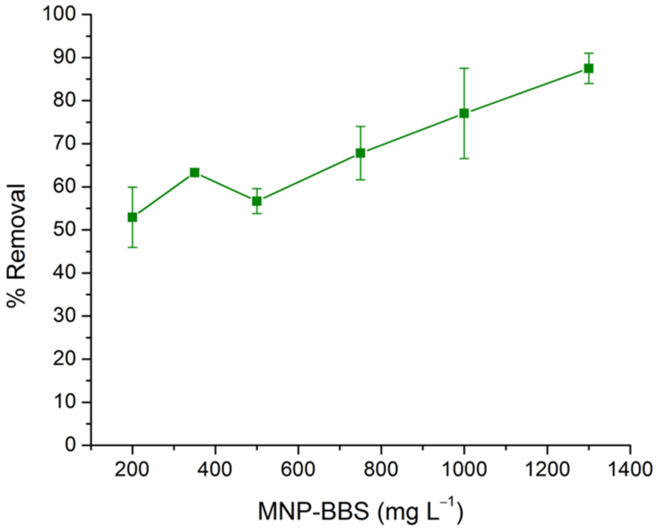

Figure 6. Effect of adsorbent concentration on PQ removal in the range of 200 to 1300 mg L^{-1} at pH 6.2.

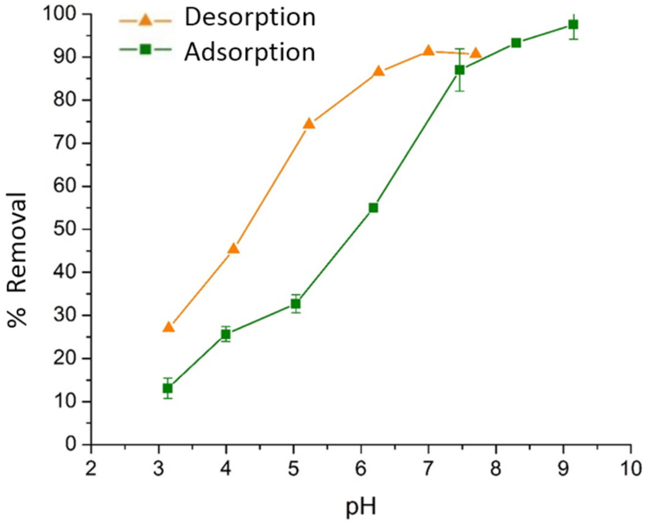

Figure 7. % Removal obtained with MNP-BBS at different pH values (Adsorption). Desorption of PQ induced by decreasing the pH from MNP-BBS with adsorbed PQ at pH 8 (Desorption). [MNP-BBS] = 500 mg L^{-1}, [PQ] = 3 mg L^{-1}.

In addition to assessing the effect of pH on adsorption, we aimed to investigate the nature of the interaction between PQ and MNP-BBS, as well as the competition with H^+. To achieve this, an experiment was conducted where the desorption of PQ was induced by progressively increasing the concentration of H^+ in an initial system of MNP-BBS previously in equilibrium with PQ at pH 8. A small amount of H_2SO_4 was added to the system, which was then stirred for 30 min, and an aliquot was withdrawn and separated using a magnet. This process was repeated by continuously adding acid and withdrawing aliquots until the system reached a progressive decrease in pH down to 3. In this way, a desorption PQ from the MNP-BBS surface is induced by decreasing the pH of the medium. Comparing both curves in Figure 7 (i.e., adsorption and desorption), it is evident that the amount of PQ retained on the adsorbent differ, indicating that the adsorption process is not entirely reversible. In particular, higher PQ amounts remains adsorbed onto MNP-BBS after decreasing the pH (desorption) compared to the adsorbed PQ in the adsorption experiments at the same pH value. This behavior suggests that the PQ adsorbed on the surface of MNP-

BBS is not easily displaced by protons from the medium and that the electrostatic attractions between PQ and BBS are not the only mode of interaction between the herbicide and the adsorbent. Therefore, contributions from π-π interactions and hydrophobic interactions with non-ionizable groups could also participate in the adsorption mechanism.

The effect of the ionic strength of the medium was studied by carrying out experiments in the presence of different amounts of NaCl and $CaCl_2$ independently (Figure 8). The presence of NaCl appears to have no significant effect on the retention of the contaminant. However, $CaCl_2$ has a substantial negative impact on the adsorption of PQ, reducing the removal capacity from 55% to 15% in the presence of 0.01 M $CaCl_2$. This reduction in adsorption is explained by the fact that Ca^{2+} competes with paraquat for adsorption sites. This is consistent with previous reports on the interaction between PQ and soil organic matter in the presence of Ca^{2+} [30]. Bivalent cations, such as Ca^{2+}, are known to exhibit a higher affinity for carboxyl groups compared to monovalent ions. Thus, these findings support the hypothesis that PQ interacts with the carboxyl groups of BBS on the surface of the nanoparticles.

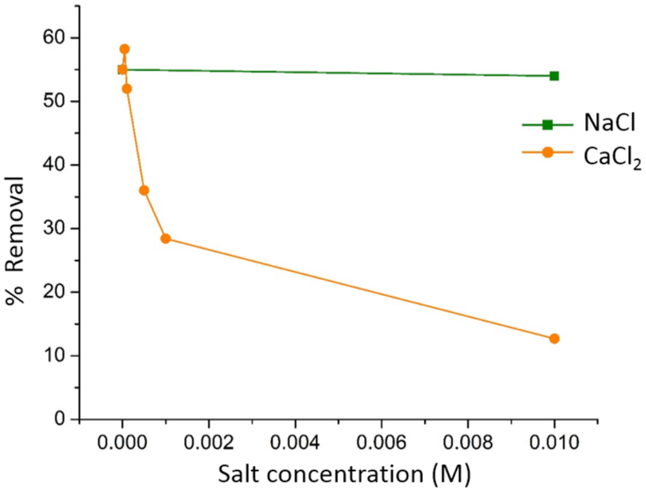

Figure 8. Effect of NaCl and $CaCl_2$ on % Removal. [MNP-BBS] = 500 mg L^{-1}, [PQ] = 3 mg L^{-1}, pH = 6.2.

Figure 9 shows the PQ adsorption isotherm obtained at room temperature and pH 6.75. The experiments were conducted by maintaining the MNP-BBS concentration constant at 500 mg L^{-1} while varying the initial PQ concentration from 1 to 75 mg L^{-1}. The amount of PQ retained increases with the increasing concentration of the pesticide in solution. The obtained results were fitted to the Langmuir and Freundlich models. The parameters of each model and the quality of the fit are presented in Table 2. The values of R^2 suggest that the data better fit Freundlich model. The value of $n > 1$ would indicate a high affinity for the adsorbent. This result also suggests a high heterogeneity of active sites on the adsorbent, and as consequence, the possibility of interaction with PQ through different mechanisms. For comparative purposes, Table 2 compiles the PQ adsorption parameters with other adsorbents reported in the literature. It can be seen that the maximum PQ removal capacity (q_{max}) obtained in this work is comparable to values reported for different types of mesoporous clays and silicas. Although similar or lower q_{max} values have been obtained compared to other adsorbents, the magnetic properties of NP-STH allow for simple and inexpensive separation of the nanomaterials.

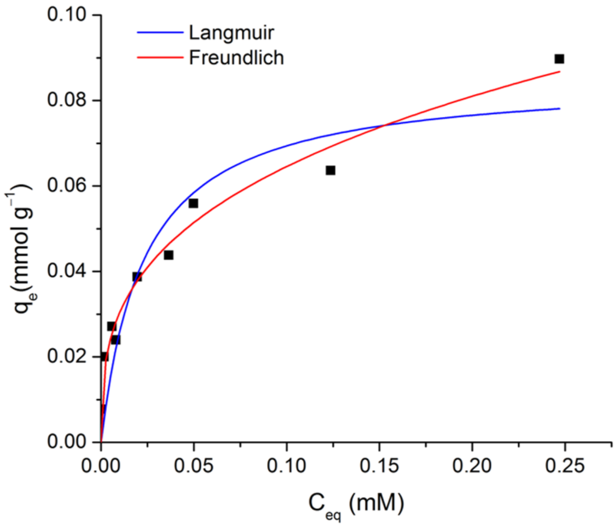

Figure 9. Adsorption isotherm of PQ on MNP-BBS. [MNP-BBS] = 500 mg L^{-1}, pH = 6.75, T = 25 °C. The blue and red lines show the fitting of the experimental data using Langmuir and Freundlich models, respectively.

Table 2. Langmuir and Freundlich isothermal adsorption parameters for the adsorption of PQ by MNP-BBS. For comparison purpose, PQ adsorption parameters with other adsorbents reported in the literature.

Adsorbents	**Langmuir Model**			**Freundlich Model**			**Ref.**
	q_{max} **(mmol g^{-1})**	K_L **(mmol^{-1})**	R^2	K_F **(L^{-1} mmol$^{(n-1/n)}$ g^{-1})**	n	R^2	
MNP-BBS	0.085	43	0.86	0.13	3.05	0.96	this work
Sepiolite	0.048	411	0.91	0.07	6.94	-	[31]
Bentonite	0.0165	732	0.99	0.19	15	-	[31]
SBA-15	0.036	-	0.98				[32]
MCM-41	0.083	-	0.98				[33]
Activated carbon	0.29	5.9	0.99				[17]

4. Conclusions

In this study, magnetic iron oxide nanoparticles coated with urban composted biowaste-derived substances have proven to be an effective nanoadsorbent of paraquat from water. The pH of the medium along with the time of the magnetic separation processes resulted as key parameters for achieving effective separation of the MNP-BBS from the water medium. The nanoparticles were easily recoverable using a short period of magnetic separation time (10 min) in acidic conditions (pH values lower than 6). Likewise, effective removal of the MNP-BBS was achieved at alkaline pH values but with long magnetic separation times (24 h). In the adsorption experiments, a significant effect of pH on the removal capacity of PQ was observed, with low removal at acidic pH and retention exceeding 80% at pH values higher than 7. The presence of divalent cations such as Ca^{2+} had a negative impact on PQ removal due to competition for active BBS sites from nanoparticles. The results obtained suggested that the adsorption mechanism mainly involves electrostatic interactions between the negative functional groups of the adsorbent and the organic cation PQ. However, other types of interaction such as π-π and hydrophobic interactions may also contribute to the adsorption of PQ. The equilibrium experimental data displayed a high adsorption performance with a good fit to the Freundlich isotherm model. The high efficiency of PQ removal, together with the magnetic properties displayed by these nanomaterials, clearly demonstrate that MNP-BBS can be successfully used as a green, sustainable, versatile and low-cost adsorbent for the remediation of PQ-contaminated waters.

Author Contributions: Conceptualization, M.E.P. and L.C.; methodology, S.O. and L.C.; investigation, S.O.; writing—original draft preparation, M.E.P., S.O. and L.C.; writing—review and editing, M.E.P. and L.C.; project administration, M.E.P. and L.C.; funding acquisition, M.E.P. and L.C. All authors have read and agreed to the published version of the manuscript.

Funding: This research was funded by ANPCyT (PICT-1847-2017), UNCo (PIP 04/L009), and CONICET (PIP 11220200100768CO).

Data Availability Statement: Data is contained within the article.

Acknowledgments: The authors are especially grateful to Giuliana Magnacca (University of Turin) for providing BBS substances. S.O. thanks the CONICET for his research graduate grant. L.C. is a research member of CONICET.

Conflicts of Interest: The authors declare no conflict of interest.

References

1. Loewy, R.M.; Monza, L.B.; Kirs, V.E.; Savini, M.C. Pesticide Distribution in an Agricultural Environment in Argentina. *J. Environ. Sci. Health Part B* **2011**, *46*, 37–41.
2. Gensch, L.; Jantke, K.; Rasche, L.; Schneider, U.A. Pesticide Risk Assessment in European Agriculture: Distribution Patterns, Ban-Substitution Effects and Regulatory Implications. *Environ. Pollut.* **2024**, *348*, 123836. [CrossRef] [PubMed]
3. Islam, M.A.; Amin, S.M.N.; Rahman, M.A.; Juraimi, A.S.; Uddin, M.K.; Brown, C.L.; Arshad, A. Chronic Effects of Organic Pesticides on the Aquatic Environment and Human Health: A Review. *Environ. Nanotechnol. Monit. Manag.* **2022**, *18*, 100740. [CrossRef]
4. Peña-Acevedo, L.M.; Ballesteros-Castro, D.A.; Sukumar, C.A. Paraquat. *Encycl. Toxicol. Fourth Ed.* **2023**, *7*, 269–281. [CrossRef]
5. Donley, N. The USA Lags behind other Agricultural Nations in Banning Harmful Pesticides. *Environ. Health* **2019**, *18*, 44. [CrossRef]
6. Franco, D.S.P.; Georgin, J.; Lima, E.C.; Silva, L.F.O. Advances Made in Removing Paraquat Herbicide by Adsorption Technology: A Review. *J. Water Process. Eng.* **2022**, *49*, 102988. [CrossRef]
7. Adeleye, A.S.; Conway, J.R.; Garner, K.; Huang, Y.; Su, Y.; Keller, A.A. Engineered Nanomaterials for Water Treatment and Remediation: Costs, Benefits, and Applicability. *Chem. Eng. J.* **2016**, *286*, 640–662. [CrossRef]
8. Xu, P.; Zeng, G.M.; Huang, D.L.; Feng, C.L.; Hu, S.; Zhao, M.H.; Lai, C.; Wei, Z.; Huang, C.; Xie, G.X.; et al. Use of Iron Oxide Nanomaterials in Wastewater Treatment: A Review. *Sci. Total Environ.* **2012**, *424*, 1–10. [CrossRef] [PubMed]
9. Gómez-Pastora, J.; Bringas, E.; Ortiz, I. Recent Progress and Future Challenges on the Use of High Performance Magnetic Nano-Adsorbents in Environmental Applications. *Chem. Eng. J.* **2014**, *256*, 187–204. [CrossRef]
10. Peralta, M.E.; Ocampo, S.; Funes, I.G.; Medina, F.O.; Parolo, M.E.; Carlos, L. Nanomaterials with Tailored Magnetic Properties as Adsorbents of Organic Pollutants from Wastewaters. *Inorganics* **2020**, *8*, 24. [CrossRef]
11. Ananpattarachai, J.; Aphaiphak, P.; Ard-Ong, R.; Kajitvichyanukul, P.; Hung, Y.T. Adsorption Isotherm and Kinetics of Paraquat Removal Using Activated Carbon/Iron Oxide Composite Material. *Int. J. Environ. Waste Manag.* **2016**, *17*, 189–202. [CrossRef]
12. Fernandes, T.; Soares, S.F.; Trindade, T.; Daniel-Da-silva, A.L. Magnetic Hybrid Nanosorbents for the Uptake of Paraquat from Water. *Nanomaterials* **2017**, *7*, 68. [CrossRef]
13. Ahmad, F.A. The Use of Agro-Waste-Based Adsorbents as Sustainable, Renewable, and Low-Cost Alternatives for the Removal of Ibuprofen and Carbamazepine from Water. *Heliyon* **2023**, *9*, e16449. [CrossRef] [PubMed]
14. Hu, J.; Zhao, L.; Luo, J.; Gong, H.; Zhu, N. A Sustainable Reuse Strategy of Converting Waste Activated Sludge into Biochar for Contaminants Removal from Water: Modifications, Applications and Perspectives. *J. Hazard. Mater.* **2022**, *438*, 129437. [CrossRef]
15. Li, J.; Liu, Y.; Wang, J.; Liu, Y.; Zhang, M.; Zhao, L.; Gu, S.; Lin, R.; Chen, L. Research Progress on the Application of Natural Adsorbents in the Treatment of Livestock Wastewater. *Desalination Water Treat* **2024**, *317*, 100018. [CrossRef]
16. Tsoutsa, E.K.; Tolkou, A.K.; Kyzas, G.Z.; Katsoyiannis, I.A. An Update on Agricultural Wastes Used as Natural Adsorbents or Coagulants in Single or Combined Systems for the Removal of Dyes from Wastewater. *Water Air Soil Pollut.* **2024**, *235*, 178. [CrossRef]
17. Hamadi, N.K.; Swaminathan, S.; Chen, X.D. Adsorption of Paraquat dichloride from aqueous solution by activated carbon derived from used tires. *J. Hazard. Mater.* **2004**, *112*, 133–141. [CrossRef]
18. Damdib, S.; Siyasukh, A.; Vanichsetakul, B.; Phamornpiboon, P.; Thanachayanont, C.; Punyapalakul, P.; Tonanon, N. Efficient Removal of Paraquat Pollutants Using Magnetic Biochar Derived from Corn Husk Waste: A Sustainable Approach for Water Remediation. *Adsorpt Sci. Technol.* **2023**, *2023*, 5512881.
19. Nisticò, R.; Celi, L.R.; Bianco Prevot, A.; Carlos, L.; Magnacca, G.; Zanzo, E.; Martin, M. Sustainable Magnet-Responsive Nanomaterials for the Removal of Arsenic from Contaminated Water. *J. Hazard. Mater.* **2018**, *342*, 260–269. [CrossRef]
20. Nisticò, R.; Cesano, F.; Franzoso, F.; Magnacca, G.; Scarano, D.; Funes, I.G.; Carlos, L.; Parolo, M.E. From Biowaste to Magnet-Responsive Materials for Water Remediation from Polycyclic Aromatic Hydrocarbons. *Chemosphere* **2018**, *202*, 686–693. [CrossRef] [PubMed]

21. Magnacca, G.; Allera, A.; Montoneri, E.; Celi, L.; Benito, D.E.; Gagliardi, L.G.; Gonzalez, M.C.; Mártire, D.O.; Carlos, L. Novel Magnetite Nanoparticles Coated with Waste-Sourced Biobased Substances as Sustainable and Renewable Adsorbing Materials. *ACS Sustain. Chem. Eng.* **2014**, *2*, 1518–1524. [CrossRef]
22. Nisticò, R.; Barrasso, M.; Carrillo Le Roux, G.A.; Seckler, M.M.; Sousa, W.; Malandrino, M.; Magnacca, G. Biopolymers from Composted Biowaste as Stabilizers for the Synthesis of Spherical and Homogeneously Sized Silver Nanoparticles for Textile Applications on Natural Fibers. *ChemPhysChem* **2015**, *16*, 3902–3909. [CrossRef] [PubMed]
23. Vargas, J.M.; Shukla, D.K.; Meneses, C.T.; Mendoza Zélis, P.; Singh, M.; Sharma, S.K. Synthesis, Phase Composition, Mössbauer and Magnetic Characterization of Iron Oxide Nanoparticles. *Phys. Chem. Chem. Phys.* **2016**, *18*, 9561–9568.
24. Yamaura, M.; Camilo, R.L.; Sampaio, L.C.; Macêdo, M.A.; Nakamura, M.; Toma, H.E. Preparation and characterization of (3-aminopropyl)triethoxysilane-coated magnetite nanoparticles. *J. Magn. Magn. Mater.* **2004**, *279*, 210–217. [CrossRef]
25. Ou, X.; Chen, S.; Quan, X.; Zhao, H. Photochemical Activity and Characterization of the Complex of Humic Acids with Iron(III). *J. Geochem. Explor.* **2009**, *102*, 49–55. [CrossRef]
26. Gu, B.; Chen, Z.; Mccarthyt, J.F.; Divlslon, E.S.; Division, C.; Ridge, O. Adsorption and Desorption of Natural Organic Matter on Iron Oxide: Mechanisms and Models. *Environ. Sci. Technol.* **1994**, *28*, 38–46. [CrossRef] [PubMed]
27. Agmo Hernández, V. An overview of surface forces and the DLVO theory. *ChemTexts* **2023**, *9*, 10. [CrossRef]
28. Stephens, J.R.; Beveridge, J.S.; Williams, M.E. Analytical Methods for Separating and Isolating Magnetic Nanoparticles. *Phys. Chem. Chem. Phys.* **2012**, *14*, 3280–3289. [CrossRef] [PubMed]
29. Iglesias, A.; López, R.; Gondar, D.; Antelo, J.; Fiol, S.; Arce, F. Effect of pH and Ionic Strength on the Binding of Paraquat and MCPA by Soil Fulvic and Humic Acids. *Chemosphere* **2009**, *76*, 107–113. [CrossRef] [PubMed]
30. Gondar, D.; López, R.; Antelo, J.; Fiol, S.; Arce, F. Adsorption of Paraquat on Soil Organic Matter: Effect of Exchangeable Cations and Dissolved Organic Carbon. *J. Hazard. Mater.* **2012**, *235–236*, 218–223. [CrossRef]
31. Seki, Y.; Yurdakoç, K. Paraquat Adsorption onto Clays and Organoclays from Aqueous Solution. *J. Colloid Interface Sci.* **2005**, *287*, 1–5. [CrossRef]
32. Osakoo, N.; Pansakdanon, C.; Sosa, N.; Deekamwong, K.; Keawkumay, C.; Rongchapo, W.; Chanlek, N.; Jitcharoen, J.; Prayoonpokarach, S.; Wittayakun, J. Characterization and Comprehension of Zeolite NaY/Mesoporous SBA-15 Composite as Adsorbent for Paraquat. *Mater. Chem. Phys.* **2017**, *193*, 470–476. [CrossRef]
33. Rongchapo, W.; Sophiphun, O.; Rintramee, K.; Prayoonpokarach, S.; Wittayakun, J. Paraquat Adsorption on Porous Materials Synthesized from Rice Husk Silica. *Water Sci. Technol.* **2013**, *68*, 863–869. [CrossRef] [PubMed]